

ORIGINAL ARTICLE

Open Access



Preliminary clinical assessment of dynamic carbon-11 methionine positron-emission tomography/computed tomography for the diagnosis of the pathologies in patients with musculoskeletal lesions: a prospective study

Takayoshi Shinya^{1,2,3*} , Yoichi Otomi¹, Toshihiko Nishisho⁴, Bettina Beuthien-Baumann², Michiko Kubo¹, Hideki Otsuka⁵, Yoshimi Bando⁶, Hiroaki Yanagawa⁷, Koichi Sairyō⁴ and Masafumi Harada¹

* Correspondence: midnight-2005@nifty.com

¹Department of Radiology, Tokushima University Hospital, 2-50-1, Kuramoto-cho, Tokushima City, Tokushima 770-8503, Japan

²Division of Radiology, German Cancer Research Centre (DKFZ), Im Neuenheimer Feld 280, 69120 Heidelberg, Germany

Full list of author information is available at the end of the article

Abstract

Background: This study prospectively assessed the diagnostic capacity of dynamic carbon-11 methionine (C-11 MET) positron-emission tomography (PET)/computed tomography for the diagnosis of pathologies in patients with primary unknown musculoskeletal lesions (MSLs). In total, 13 patients with MSLs underwent dynamic scans (5–10 [phase 1], 10–15 [phase 2], 15–20 [phase 3], 20–25 [phase 4], 25–30 [phase 5], and 30–35 [phase 6] min post-injection of C-11 MET). We statistically compared the maximum standardised uptake values (SUVmax) and corresponding retention index for dynamic scans (RI-SUV) for five benign MSLs (BMSLs), five primary malignant musculoskeletal tumours (PMMSTs), four metastatic musculoskeletal tumours (MMSTs), and three malignant lymphoma (ML) cases and explored their diagnostic capacities using receiver operating characteristic (ROC) curve analyses.

Results: SUVmax gradually decreased or remained similar with minimal fluctuations in all BMSL cases and four of five PMMST cases. In contrast, SUVmax increased over time in one case of PMMST and in all cases of MMST and ML. Significant differences were observed in SUVmax for all time phases and RI-SUV between BMSLs and MMSLs, in SUVmax for all time phases between PMMSTs and BMSLs, in SUVmax for all time phases and RI-SUV between non-PMMST-malignant tumours and BMSL, and in RI-SUV between non-PMMST-malignant tumours and PMMST. In ROC analyses, the areas under the curve yielded the highest values at 1.00 for differentiating most intergroup comparisons.

Conclusions: Dynamic C-11 MET PET scans have the potential to be good predictors of discriminating MSLs in patients with primary unknown MSLs in clinical practice.

Keywords: Musculoskeletal lesion, Sarcoma, Malignant lymphoma, Diagnostic validity, C-11 MET, Dynamic PET/CT, SUVmax

Background

Musculoskeletal lesions (MSLs) constitute a wide range of physiological, biochemical, and genetic characteristics. In clinical practice, orthopaedic surgeons and radiologists encounter pathologically unknown MSLs. It is of major diagnostic importance to differentiate between a benign musculoskeletal lesion (BMSL) and malignancy from the aspects of indication for biopsy and determining optimal treatment. Moreover, differentiating MSLs with morphologic imaging such as conventional radiography, computed tomography (CT), and magnetic resonance imaging may result in the diagnostic dilemma of differential diagnosis due to non-specific features and considerable overlap with other pathologies in cases with atypical image findings (Fletcher et al., 2002; Raphael et al., 2013; Lim et al., 2013).

Functional imaging techniques, including thallium-201 (^{201}Tl) scintigraphy, $^{99\text{m}}\text{Tc}$ (V) dimercaptosuccinic acid scintigraphy, and fluorine-18-fluorodeoxyglucose (^{18}F -FDG) positron emission tomography/computed tomography (PET/CT), are increasingly being used to obtain complementary information in specific clinical situations (Inai et al., 2015; Keller et al., 2017; Kobayashi et al., 1995; Choong et al., 2004; Shinya et al., 2015; Hicks, 2005). However, even with metabolic imaging including ^{18}F -FDG PET/CT, there are overlapping features among MSLs. One limitation is the relatively high rate of false-positive results caused by inflammatory tissues. Therefore, the development of post- ^{18}F -FDG molecular probes such as carbon-11 methionine (^{11}C -MET), which reflects increased amino acid transport and protein synthesis and is related to cellular proliferation activity, is expected to overcome these problems (van Waarde et al., 2006).

Absolute PET quantification of physiological parameters via tracer kinetic modelling and dynamic PET imaging is expected to facilitate elucidation of the pathophysiological mechanisms of histology and extraction of physiological or biochemical parameters via tracer kinetics (Dimitrakopoulou-Strauss et al., 2001; Dimitrakopoulou-Strauss et al., 2002; Rusten et al., 2013; Okazumi et al., 2009; Dimitrakopoulou-Strauss et al., 2010a; Dimitrakopoulou-Strauss et al., 2010b). Despite its availability, dynamic PET imaging with kinetic model analysis has been primarily confined to research centres and has not been used in busy clinical settings, mainly due to time-demanding imaging protocols and sophisticated evaluation tools for the evaluation of dynamic scans (Kwee et al., 2010). Nevertheless, technical developments in dynamic ^{18}F -FDG PET/CT have enabled the investigation of perfusion-dependent FDG uptake and metabolic activity in various tumour entities (Schierz et al., 2013; Bernstine et al., 2011; Epelbaum et al., 2013; Belakhlef et al., 2012; Nakajima et al., 2016). Recent studies have performed dynamic PET/CT in list-mode without kinetic model analysis as a simple method to predict pathological and clinicopathological findings of tumours (Schierz et al., 2013; Nakajima et al., 2016; Shinya et al., 2019; Shinya et al., 2020). In a study using small animal PET analysis, Zhao et al. demonstrated that the dynamic pattern of ^{11}C -MET uptake was significantly different between granulomas and tumours (Zhao et al., 2011). In another paper on brain tumours, dynamic changes in ^{11}C -MET uptake varied between different tumour pathologies, and ^{11}C -MET PET imaging revealed additional information to differentiate brain tumours (Aki et al., 2012). However, to our knowledge, no study to date has assessed the diagnostic capacity of dynamic ^{11}C -MET PET/CT for differentiating between BMSL and malignant musculoskeletal lesions (MMSLs) and for differential diagnosis in MSL.

This prospective study assessed the transitional patterns of ^{11}C -MET uptake in each type of MSL, which include BMSLs, primary malignant musculoskeletal tumours

(PMMSTs), metastatic musculoskeletal tumours (MMSTs), and malignant lymphomas (MLs), on dynamic scans and investigated the diagnostic capacity of dynamic ^{11}C -MET PET/CT with list-mode for the differentiation of patients with primary unknown MSLs.

Methods

Study population

This single-centre prospective study was approved by our institutional review board and ethics committee. A written informed consent form was signed by all patients. All procedures for studies involving human participants were conducted in accordance with the 1964 Helsinki Declaration and its later amendments or comparable ethical standards. We included patients older than 20 years with pathologically unknown MSL, in whom diagnosis was finally determined on pathologic examination; patients who had not undergone therapy for MSL before PET/CT; and patients without malignancy within the last 5 years.

^{11}C -Methionine PET/CT procedures

The PET study was performed according to standardised procedures. A dose of 3.7 MBq/kg MET was injected intravenously. PET/CT imaging was conducted using a single PET/CT system (Discovery PET/CT 710; GE Healthcare, Chicago, IL, USA), which had list-mode data acquisition and enabled four-dimensional data acquisition (i.e. dynamic studies). The protocol included the following two PET/CT acquisitions: (1) a dynamic PET acquisition (limited to the single bed position) and (2) a low-dose CT scan centred on the largest MSL of interest and initiated 5 min after the intravenous injection of ^{11}C -MET. All participants underwent dynamic PET/CT examinations.

In the first acquisition, low-dose CT was acquired for PET attenuation correction, anatomical information, and image fusion. In the second acquisition, dynamic ^{11}C -MET PET/CT imaging was conducted as list-mode continuous scanning with every measured value stored as raw data with exact time stamps beginning at 5 min after the MET bolus and continuing for 30 min. The dynamic series was acquired with the field of view over the lesions of interest (limited to a single bed position, with the coverage in the patient's longitudinal direction of 15.042 cm). Patients were instructed to lie motionless for the duration of the dynamic study. We subsequently reconstructed the data as six frames at 300-s intervals. The list-mode files were reconstructed on the PET/CT scanner. The frames were reconstructed using three-dimensional attenuation-weighted ordered-subset expectation maximisation with two iterations and 16 subsets (VUE Point FX; GE Healthcare) with 4-mm post reconstruction Gaussian filter, attenuation image segmentation, and a 192×192 pixel matrix.

Analysis of PET/CT images

The dynamic PET/CT images were reviewed by two nuclear medicine physicians with 19 and 17 years of experience, respectively. Both readers were blinded to all clinical, pathological, and other imaging findings. If the results of the two physicians differed, they discussed the findings until a consensus was reached. Any obvious foci of MET uptake within MSLs that were increased relative to the surrounding tissue that was unrelated to physiologic sites of tracer uptake were considered positive findings.

By using the PET/CT images, we carefully placed the volume of interest (VOI) on the MSL to exclude MET accumulation in normal tissue and large vessels. Circular VOIs

were drawn to encompass each lesion contour on transaxial images. VOIs were placed by consensus between the two nuclear medicine physicians.

For semiquantitative analysis of MET uptake, we adopted the standardised uptake value (SUV). The SUVs were calculated using lean body mass, as follows:

$$\text{SUV} = \text{concentration of radioactivity (Bq/kg)} \times [\text{body mass (kg)}/\text{injected radioactivity (Bq)}]$$

To minimise partial-volume effects, the SUVmax within the VOIs was used for the statistical analyses. The SUVmax was measured for each dynamic phase (i.e. SUV1, 5–10 min; SUV2, 10–15 min; SUV3, 15–20 min; SUV4, 20–25 min; SUV5, 25–30 min; and SUV6, 30–35 min). Furthermore, we calculated the RI-SUV from the SUVmax, based on the following formula:

$$\text{Retention index of the phase SUVmax (RI - SUV[\%])} = (\text{SUV6} - \text{SUV1}) \times 100/\text{SUV1}$$

In addition, we calculated the mean SUV (SUVmean) for each subject.

The maximal diameter of each tumour lesion was measured on axial low-dose CT images.

Statistical analysis

The Mann-Whitney *U* test or Kruskal-Wallis test followed by the Steel-Dwass test were employed to analyse the differences in SUVmax for each of the 6 dynamic phases and RI-SUV. If the statistical test revealed a significant difference in each index among the groups of MSLs, an additional receiver operating characteristic (ROC) analysis of the SUVmax and RI-SUV was conducted to evaluate the predictive performance of calculating each index for discriminating the groups. Discrimination was assessed by using the area under the ROC curve (AUC). We determined the optimal cut-off values that maximised the sensitivity and specificity for each index and the corresponding sensitivity, specificity, positive predictive value (PPV), negative predictive value (NPV), and accuracy. Significant differences between the two AUCs, as determined from the ROC curve, were assessed with Delong's test. Statistical analyses were conducted using EZR version 1.37 (Saitama Medical Centre, Jichi Medical University, Saitama, Japan; available at www.jichi.ac.jp/saitama-sct/SaitamaHP.files/statmedEN.html) which is a graphical user interface for R (The R Foundation for Statistical Computing, Vienna, Austria) (Kanda, 2013). Statistical significance was set at $p < 0.05$.

Results

Patients and tumour characteristics

Patient and tumour characteristics are indicated in Table 1. Between February 2016 and November 2016, a total of 13 patients met the criteria for this prospective analysis and underwent dynamic ^{11}C -MET PET/CT (nine males and four females; age [mean \pm SD], 69.69 ± 10.23 ; range, 54–85 years). Seventeen lesions were interpreted as bone and soft tissue lesions on PET/CT evaluations (13 soft tissue, four bone). MSLs were classified according to the WHO Classification of Tumours of Soft Tissue and Bone, Fourth Edition, by pathologists blinded to PET results (Fletcher et al., 2013).

The 17 lesions were assigned to 4 groups: BMSLs ($n = 5$, 29%), PMMSTs ($n = 5$, 29%), MMSTs ($n = 4$, 24%), and MLs ($n = 3$, 18%). The tumour sizes ranged from 20

Table 1 Characteristics of patients and tumours

No./patient no./age/sex	Histology	Tumour site	Diameter (mm)
A. Benign musculoskeletal lesion			
1/1/80/male	Osteochondroma	Knee	20
2/2/68/male	Osteochondroma	Knee	40
3/3/67/male	Haematoma	Femur	245
4/4/77/male	Schwannoma	Axilla	56
5/5/61/female	Schwannoma	Thigh	35
B. Primary malignant musculoskeletal tumour			
6/6/59/male	Pleomorphic leiomyosarcoma	Lower back	79
7/6/59/male	Pleomorphic leiomyosarcoma	Lower back	28
8/7/55/male	Myxofibrosarcoma	Thigh	57
9/8/81/male	Pleomorphic leiomyosarcoma	Back	48
10/9/70/male	Myxofibrosarcoma	Shoulder	66
C. Metastatic musculoskeletal tumour			
11/10/78/female	AC from gastric cancer	Thigh (muscle)	79
12/11/71/male	SCC from hypopharyngeal cancer	Neck (muscle)	21
13/11/71/male	SCC from hypopharyngeal cancer	Neck (muscle)	28
14/11/71/male	SCC from hypopharyngeal cancer	Neck (muscle)	23
D. Malignant lymphoma			
15/12/54/female	Diffuse large B cell lymphoma	Sacrum	87
16/13/85/female	Diffuse large B cell lymphoma	Thigh	57
17/13/85/female	Diffuse large B cell lymphoma	Thigh	20

AC adenocarcinoma, SCC squamous cell carcinoma

to 245 mm, with most lesions < 70 mm in long-axis diameter. There were no significant differences in tumour size among groups ($p = 0.697$).

Standardised uptake values and retention index of maximum SUV

SUVmax, RI-SUV values, and SUVmean are summarised in Tables 2 and 3. Figure 1 shows the change in median SUVmax values for each time phase per study group. SUVmax values decreased gradually or remained relatively stable with minimal fluctuations in all BMSL cases and four of five PMMST cases. In contrast, SUVmax values progressively increased over time in one PMMST case (case no. 9), in which round and polymorphic tumour cells are more densely growing compared with the other two pleomorphic leiomyosarcomas with myxomatous components (case no. 6 and no. 7) and all MMST and ML cases.

All metabolic parameters were significantly higher in MMSLs than in BMSLs ($p < 0.001$ for all SUVmax; $p = 0.0194$ for RI-SUV). The SUVmax values for each time phase were significantly higher for PMMST than for BMSL ($p = 0.00471$ for all SUVmax values). In contrast, no significant differences were detected in RI-SUV between PMMSTs and BMSLs ($p = 0.78327$) or in all parameters between other single groups.

Values of all metabolic parameters were significantly higher for non-PMMST-malignant tumours (i.e. MMSTs and MLs) than for BMSL (each p value = 0.01246). RI-SUV values were significantly higher for non-PMMST-malignant tumours than for PMMSTs

Table 2 SUVmax and RI-SUV at each time point in each group

Group	BMSL	MMSL	PMMST	MMST	ML	MMST and ML
SUV1	2.58 ± 0.50 (1.13–3.73)	6.04 ± 0.66 (4.36–11.42)	5.00 ± 0.75 (4.36–8.51)	6.04 ± 0.49 (4.86–8.51)	10.09 ± 1.12 (7.59–11.42)	7.15 ± 0.90 (4.86–11.42)
SUV2	2.18 ± 0.42 (1.07–3.41)	6.35 ± 0.89 (4.19–13.45)	4.41 ± 1.03 (4.19–9.58)	6.35 ± 0.53 (5.63–8.09)	11.91 ± 1.34 (8.90–13.45)	8.09 ± 1.13 (5.63–13.45)
SUV3	1.77 ± 0.34 (1.00–2.97)	6.69 ± 1.05 (3.57–14.90)	4.30 ± 1.11 (3.57–9.66)	6.69 ± 0.63 (6.33–9.03)	13.52 ± 1.85 (8.80–14.90)	8.80 ± 1.31 (6.33–14.90)
SUV4	1.56 ± 0.32 (1.01–2.86)	7.27 ± 1.08 (3.53–14.80)	4.25 ± 1.22 (3.53–10.13)	7.27 ± 0.89 (6.23–10.28)	13.57 ± 1.59 (9.55–14.80)	9.55 ± 1.25 (6.23–14.80)
SUV5	1.49 ± 0.27 (1.11–2.62)	7.81 ± 1.28 (3.38–18.49)	4.39 ± 1.33 (3.38–10.72)	7.81 ± 0.88 (6.97–10.94)	13.21 ± 2.44 (10.14–18.49)	10.14 ± 1.53 (6.97–18.49)
SUV6	1.41 ± 0.30 (1.03–2.75)	8.41 ± 1.26 (3.47–17.21)	4.22 ± 1.24 (3.47–10.23)	8.41 ± 0.84 (7.63–11.34)	15.07 ± 2.23 (9.72–17.21)	9.72 ± 1.40 (7.63–17.21)
RI-SUV	– 26.27 ± 12.55 (– 50.00 to 23.6)	30.01 ± 9.34 (– 28.89 to 70.57)	– 7.11 ± 8.06 (– 28.89 to 20.21)	48.35 ± 7.29 (34.57–63.79)	31.96 ± 13.57 (28.06–70.57)	38.10 ± 6.53 (28.06–70.57)

The data represent the median ± standard error of the mean; data in parentheses are the ranges
SUV standardised uptake value, *RI-SUV* retention index of maximum standardised uptake value, *BMSL* benign musculoskeletal lesion, *MMSL* malignant musculoskeletal lesion, *PMMST* primary malignant musculoskeletal tumour, *MMST* metastatic musculoskeletal tumour, *ML* malignant lymphoma

($p = 0.01246$). Figures 2, 3, 4, and 5 show representative dynamic ^{11}C -MET PET/CT images of each pathology.

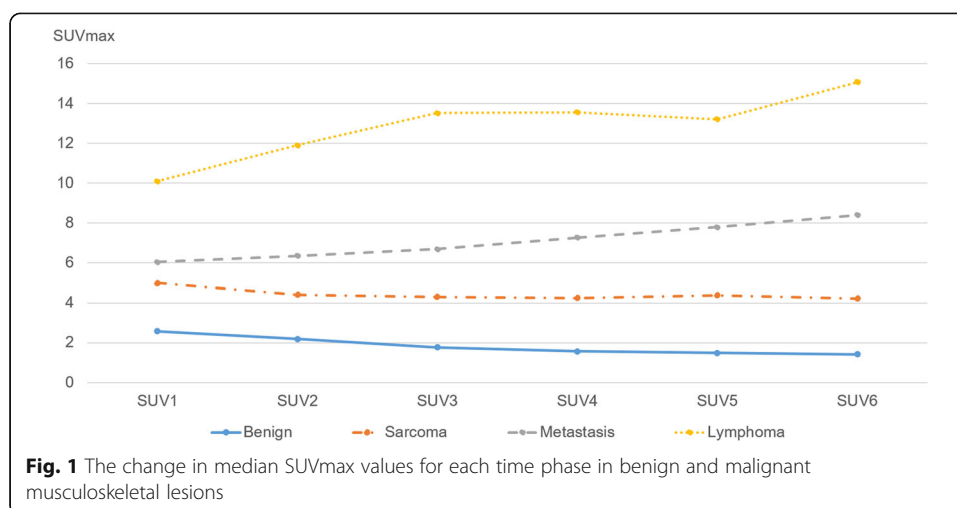
ROC curves and cut-off values for SUVmax and RI-SUV

Table 3 shows the threshold (i.e. cut-off) values for each parameter and AUC for discriminating the groups. For most comparisons between groups, cut-off SUVmax values for each dynamic phase and cut-off RI-SUV yielded a sensitivity of 100.0%, specificity of 100.0%, PPV of 100.0%, NPV of 100.0%, and accuracy of 100.0% with AUCs of 1.00 (cut-off SUV value: MMSL from BMSL: SUV1 4.36, SUV2 4.19, SUV3 3.57, SUV4 3.53, SUV5 3.38, SUV6 3.47, RI-SUV – 7.11; PMST from BMSL: SUV1 4.36, SUV2 4.19, SUV3 3.57, SUV4 3.53, SUV5 3.38, SUV6 3.47; MMST and ML from BMSL: SUV1 4.86, SUV2 5.63, SUV3 6.33, SUV4 6.23, SUV5 6.97, SUV6 7.63, RI-SUV 28.06; MMST

Table 3 SUVmean at each time point in each group

Group	BMSL	MMSL	PMMST	MMST	ML	MMST and ML
SUV1	1.13 ± 0.30 (0.75–1.53)	3.69 ± 0.39 (2.55–6.21)	2.75 ± 0.46 (2.55–4.96)	3.69 ± 0.72 (2.92–6.21)	5.21 ± 0.49 (4.32–6.03)	4.32 ± 0.48 (2.92–6.21)
SUV2	1.02 ± 0.24 (0.70–1.41)	3.85 ± 0.46 (2.27–6.71)	2.56 ± 0.59 (2.27–5.39)	3.85 ± 0.80 (3.12–6.71)	5.43 ± 0.40 (5.09–6.43)	5.09 ± 0.52 (3.12–6.71)
SUV3	1.01 ± 0.21 (0.78–1.34)	3.99 ± 0.51 (2.02–7.01)	2.56 ± 0.64 (2.02–5.53)	3.99 ± 0.74 (3.64–6.83)	6.01 ± 0.56 (5.08–7.01)	5.08 ± 0.53 (3.64–7.01)
SUV4	0.94 ± 0.17 (0.77–1.34)	4.23 ± 0.54 (1.95–7.16)	2.47 ± 0.69 (1.95–5.68)	4.23 ± 0.74 (3.60–6.89)	5.98 ± 0.48 (5.56–7.16)	5.56 ± 0.53 (3.60–7.16)
SUV5	0.94 ± 0.15 (0.71–1.25)	4.51 ± 0.56 (1.86–7.17)	2.60 ± 0.74 (1.86–5.94)	4.51 ± 0.72 (3.99–7.17)	6.06 ± 0.38 (6.03–7.17)	6.03 ± 0.50 (3.99–7.17)
SUV6	0.97 ± 0.18 (0.71–1.28)	4.74 ± 0.60 (1.85–7.72)	2.45 ± 0.73 (1.85–5.87)	4.74 ± 0.76 (4.39–7.65)	6.49 ± 0.58 (5.73–7.72)	5.73 ± 0.53 (4.39–7.72)

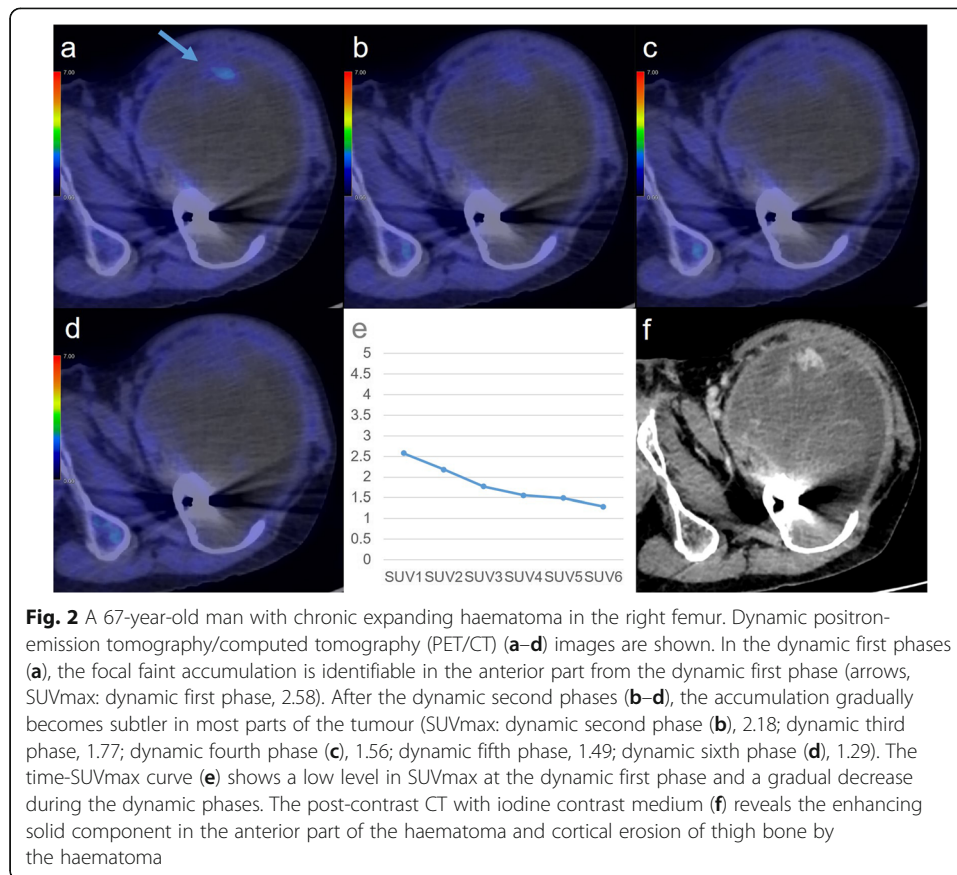
The data represent the median ± standard error of the mean; data in parentheses are the ranges
SUV standardised uptake value, *BMSL* benign musculoskeletal lesion, *MMSL* malignant musculoskeletal lesion, *PMMST* primary malignant musculoskeletal tumour, *MMST* metastatic musculoskeletal tumour, *ML* malignant lymphoma



and ML from PMMST: RI-SUV 28.06). For differentiating MMSLs and BMSLs, the cut-off RI-SUV value yielded a sensitivity of 83.3%, specificity of 80.0%, PPV of 90.9%, NPV of 66.7%, and accuracy of 82.4% with an AUC of 0.8667. Delong's test did not reveal any significant differences between the AUCs for all parameters (all $p > 0.05$).

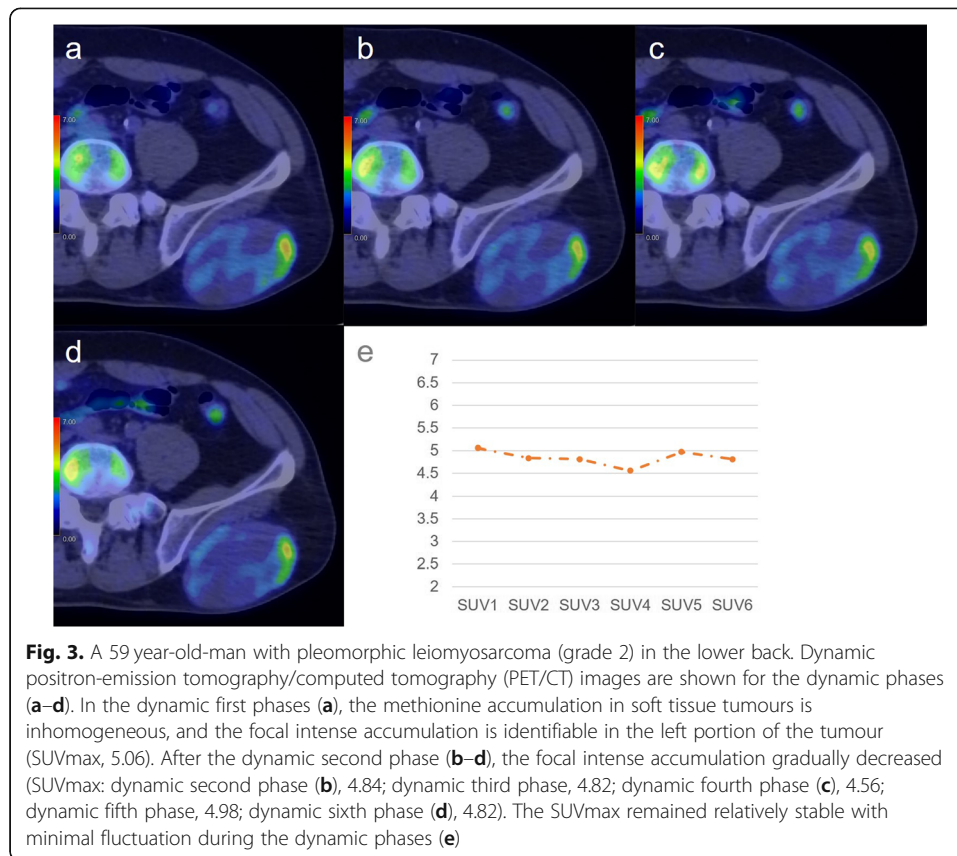
Discussion

The present study identified different dynamic changes in maximum ^{11}C -MET uptake depending on MSL histology. In all BMSL and most PMMST cases, SUVmax decreased gradually with time or remained relatively stable with minimal fluctuations. In contrast, SUVmax progressively increased over time in all MMST and ML cases and one PMMST case. In a previous study using ^{11}C -MET dynamic PET in small animals (Zhao et al., 2011), ^{11}C -MET uptake occurred faster and at a higher level in granulomas than in tumours. Further, the washout of ^{11}C -MET from the granuloma and continuous accumulation of ^{11}C -MET in the tumour were observed at later time points. In the report on a brain tumour, dynamic changes in ^{11}C -MET uptake varied between different pathologies and a significant dynamic decrease was observed in the max MET tumour-to-normal ratio in meningiomas and oligodendrocytic tumours, whereas a significant dynamic increase was observed in glioblastomas and MLs (Aki et al., 2012). In another report, Nomura et al. demonstrated MET-SUVmax increased over time during the late phase on 35-min dynamic scans in primary central nervous system lymphomas (Nomura et al., 2018). These findings could be attributed to the differences in local blood flow, stagnation of MET in the vascular beds of lesions, biological activity, cellular proliferation activity, transporters of amino acids, and enzyme activity within each lesion, degree of neovascularisation (Zhao et al., 2011; Aki et al., 2012; Okada et al., 2012). Taken together, we speculated that the strong angiogenesis and proliferation activity and the active amino acid transport mechanism or the transmethylation pathway might affect the high uptake of MET to MMST and ML in the early dynamic phase and might lead to the difference in the MET uptake to BMSL. PMMST sarcomas are composed of mesenchymal elements that contain various amounts of relatively metabolically inactive tissue such as myxoid ground substance, osteoid tissue, fluid, and necrotic tissue. They also contain a population showing varying cellularity, tissue types, and levels of dedifferentiation (Zhang et al., 2004). These might have led to the



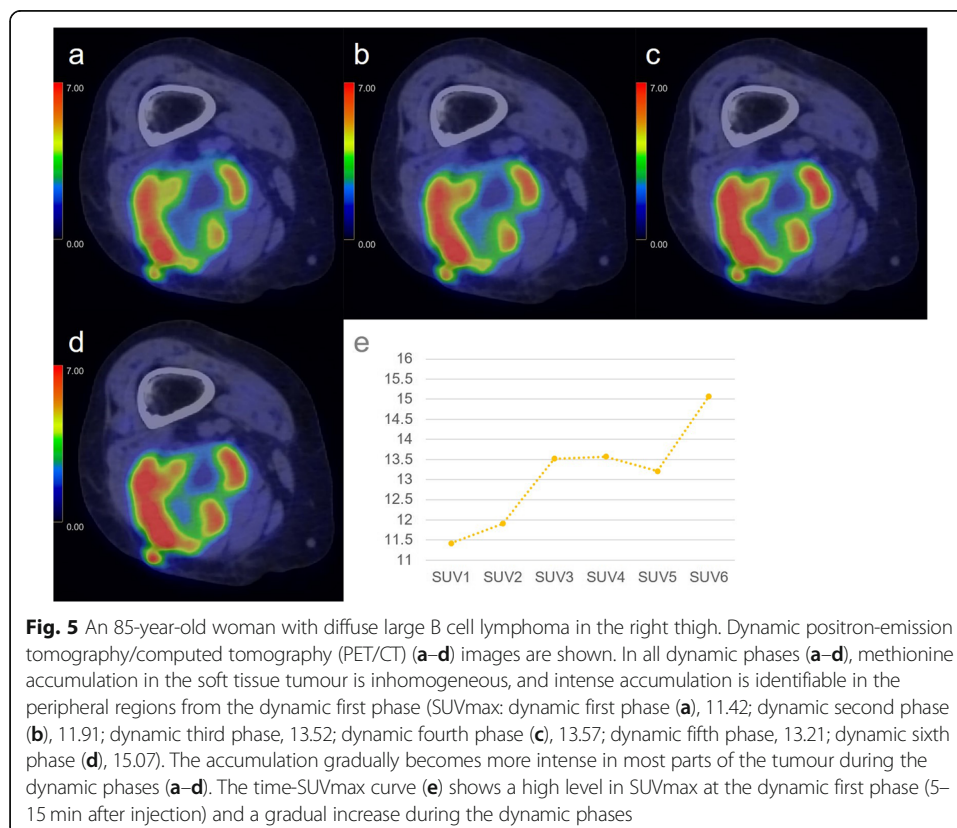
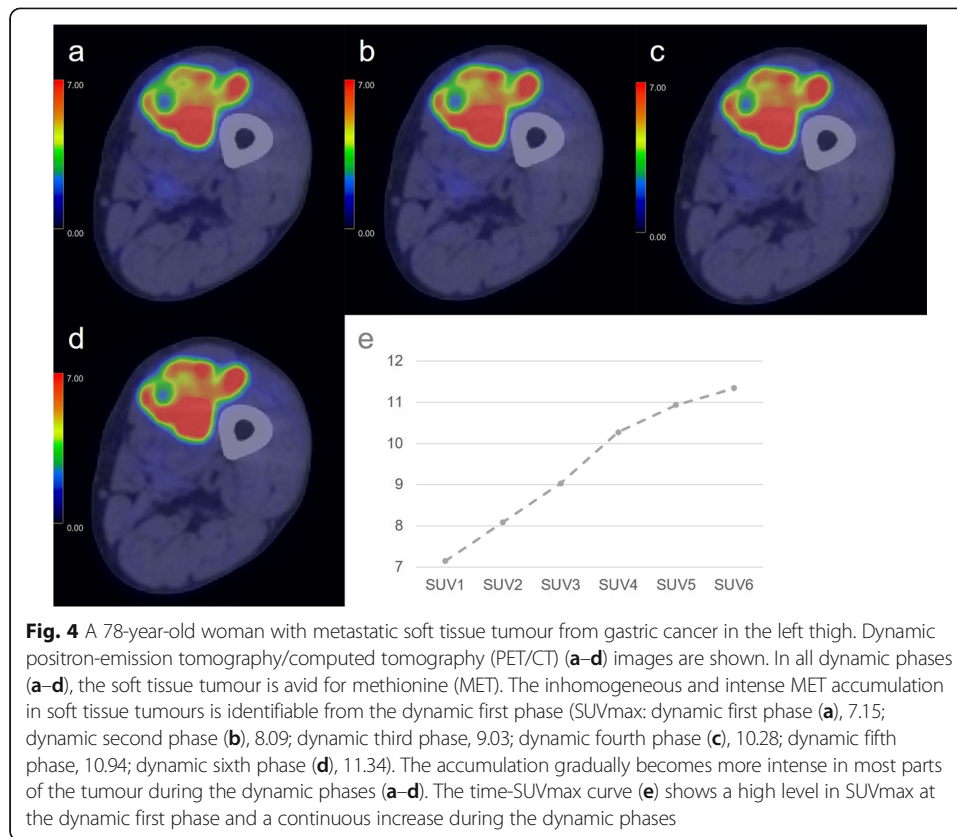
various MET uptake patterns in the present study. Therefore, the dynamic uptake patterns of ^{11}C -MET in MSLs may reveal additional information about histological and biological characteristics of different MSLs, which cannot be obtained from morphologic and static PET imaging and may be helpful for the differential diagnosis of MSLs. However, further investigation is required to reveal the mechanism and the efficiency of ^{11}C -MET PET/CT in patients with MSL lesions.

In this study, we observed that SUVmax values for each time phase were significantly higher for MMSL and PMMST than for BMSL. RI-SUV also differed significantly between BMSL and MMSL. Cut-off SUVmax values for each dynamic phase could have high diagnostic capacity in this study population, although the cut-off values in the present study are not generalisable to other institutions in clinical practice. In contrast, no significant differences were detected in other parameters between the other single groups, probably due to the small study population (four MMSL and three ML cases). However, values of all metabolic parameters were significantly higher in non-PMMST-malignant tumours (four MMST and three ML cases) than in BMSLs. RI-SUV was also significantly higher in non-PMMST-malignant tumours than in PMMSTs. A correlation between histological grade and increased MET uptake has been reported for brain, lung, and uterine tumours, and lymphomas (Derlon et al., 1989; Fujiwara et al., 1989; Lapela et al., 1994; Nuutinen et al., 1998). The MET uptake reflects the high need for amino acids for protein synthesis in cancer cells as well as enhanced trans-methylation reaction in neoplastic tissue (Nuutinen et al., 1998). These results suggested that ^{11}C -MET uptake in MSLs can differ depending on MSL histology, and ^{11}C -MET uptake in



MMSTs from adenocarcinoma and squamous cell carcinoma as well as ML (diffuse large B-cell lymphoma) can be more intense compared to that in BMSLs and PMMSTs in this study population. In addition, dynamic ^{11}C -MET PET/CT may have the diagnostic power to discriminate the histology of primary unknown MSLs with semiquantitative analyses. Dynamic ^{11}C -MET PET/CT may have the potential to aid prediction of histopathology in cases where percutaneous biopsy cannot be performed or where there are multiple sites with various suspected morphological subtypes. Moreover, recent studies have reported the efficacy of recombinant methioninase combined with palbociclib or caffeine and doxorubicin for sarcomas (Igarashi et al., 2018; Higuchi et al., 2018). Dynamic ^{11}C -MET PET/CT could be a possible biomarker for metabolic therapeutic targets in PMMSTs.

Our prospective study was limited by the small number of patients included and did not include granulomas, which show MET-avidity (false-positive) on early dynamic phases. Further, we did not assess the pathological background responsible for the difference in MET uptake into MSLs or involvement of L-type amino acid transporter 1 in the tumours, nor did we perform kinetic modelling in MET-PET. A multi-institutional trial using a larger patient population that includes each histological subtype combined with immunohistochemical analysis may provide a clearer picture and more comprehensively reveal the diagnostic capacity of dynamic ^{11}C -MET PET/CT scans for MSL. Despite its limitations, the present study identified various dynamic changes in maximum ^{11}C -MET uptake depending on the histology of the MSL and demonstrated the high diagnostic ability of this approach for the differential diagnosis of primary unknown MSLs in clinical practice with optimal cut-off levels of SUVmax



and RI-SUV. Moreover, our dynamic ^{11}C -MET PET/CT analysis can be easily obtained from dynamic PET studies with list-mode in recent clinical settings. It can be routinely performed clinically without the need for additional invasive methods, such as continuous phlebotomy for arterial input function.

Conclusion

The present study demonstrated a gradual decrease or stability with time in ^{11}C -MET uptake in BMSLs and most PMMSTs, and a transitional increase in ^{11}C -MET uptake in MMSTs and MLs. In addition, MET-avidity in MMSL was stronger than that in BMSL during all dynamic phases. The dynamic uptake patterns of ^{11}C -MET in MSLs may provide additional information about the histological and biological characteristics of different MSLs. Moreover, dynamic ^{11}C -MET PET/CT had extremely high diagnostic accuracy for differentiation of MSL using semiquantitative analyses of SUVmax and RI-SUV in the current patient population. Additional studies with more patients are needed to determine which dynamic phase is superior for differentiation in MSL.

Abbreviations

^{11}C -MET: Carbon-11 methionine; AUC: Area under the curve; BMSL: Benign musculoskeletal lesion; CT: Computed tomography; ML: Malignant lymphoma; MMSL: Malignant musculoskeletal lesions; MMST: Metastatic musculoskeletal tumour; MSL: Musculoskeletal lesion; NPV: Negative predictive value; PET: Positron-emission tomography; PMMS T: Primary malignant musculoskeletal tumour; PPV: Positive predictive value; RI-SUV: Retention index for dynamic scans; ROC: Receiving operating characteristic; SUVmax: Maximum standardised uptake values; SUVmean: Mean standardised uptake values; VOI: Volume of interest

Acknowledgements

The authors would like to thank the radiographers and administration team at Tokushima University Hospital for their technical assistance and cooperation during the imaging and administration processes.

Authors' contributions

TS is the corresponding author and participated in the writing of this paper. YO participated in the analysis of PET/CT images and performed the statistical analysis. TN, KS, and HY designed the study together with TS and provided specific suggestions to improve the manuscript. BBB, MK, HO, and MH participated in revising the manuscript and provided specific suggestions for improving it. YB performed the pathological diagnosis and pathological analysis, providing critical comments for the manuscript. All authors read and approved the final manuscript.

Funding

No funding was provided for conducting the research or for reporting the results.

Availability of data and materials

The image datasets generated and/or analysed during the current study are not publicly available due to data protection guidelines but are available from the corresponding author on reasonable request.

Ethics approval and consent to participate

All procedures performed in studies involving human participants were in accordance with the ethical standards of the institutional research committee and with the 1964 Helsinki Declaration and its later amendments or comparable ethical standards. Informed consent was obtained from all participants included in the study.

Competing interests

The authors declare that they have no competing interests.

Author details

¹Department of Radiology, Tokushima University Hospital, 2-50-1, Kuramoto-cho, Tokushima City, Tokushima 770-8503, Japan. ²Division of Radiology, German Cancer Research Centre (DKFZ), Im Neuenheimer Feld 280, 69120 Heidelberg, Germany. ³Department of Diagnostic and Therapeutic Radiology, Kawasaki Medical School General Medical Centre, 2-6-2 Nakasange, Kita-ku, Okayama City, Okayama 700-8505, Japan. ⁴Department of Orthopedics, Institute of Biomedical Sciences, Tokushima University Graduate School, 3-18-15 Kuramoto-cho, Tokushima City, Tokushima 770-8503, Japan. ⁵Department of Medical Imaging/Nuclear Medicine, Institute of Biomedical Sciences, Tokushima University Graduate School, 2-50-1, Kuramoto-cho, Tokushima City, Tokushima 770-8503, Japan. ⁶Division of Pathology, Tokushima University Hospital, 2-50-1, Kuramoto-cho, Tokushima City, Tokushima 770-8503, Japan. ⁷Clinical Trial Center for Developmental Therapeutics, Tokushima University Hospital, 2 Kuramoto-cho, Tokushima City, Tokushima 770-8503, Japan.

Received: 23 January 2020 Accepted: 21 July 2020

Published online: 26 August 2020

References

- Aki T, Nakayama N, Yonezawa S, Takenaka S, Miwa K, Asano Y et al (2012) Evaluation of brain tumors using dynamic 11C-methionine-PET. *J Neuro-Oncol* 109:115–122. <https://doi.org/10.1007/s11060-012-0873-9>
- Belakhlef S, Church C, Jani C, Lakhani S (2012) Early dynamic PET/CT and ¹⁸F-FDG blood flow imaging in bladder cancer detection: a novel approach. *Clin Nucl Med* 37:366–368
- Bernstine H, Braun M, Yefremov N, Lamash Y, Carmi R, Stern D et al (2011) FDG PET/CT early dynamic blood flow and late standardized uptake value determination in hepatocellular carcinoma. *Radiology* 260:503–510
- Choong, Kunisada T, Slaviv J, Schlicht S, Hicks R (2004) The role of thallium-201 and pentavalent dimercaptosuccinic acid for staging cartilaginous tumours. *Int Semin Surg Oncol* 1:10
- Derlon JM, Bourdet C, Bustany P, Chatel M, Theron J, Darcel F (1989) et al, [11C] L-methionine uptake in gliomas. *Neurosurgery* 25:720–729
- Dimitrakopoulou-Strauss A, Strauss LG, Egerer G, Vasamilliette J, Mechttersheimer G, Schmitt T et al (2010a) Impact of dynamic ¹⁸F-FDG PET on the early prediction of therapy outcome in patients with high-risk soft-tissue sarcomas after neoadjuvant chemotherapy: a feasibility study. *J Nucl Med* 51:551–558
- Dimitrakopoulou-Strauss A, Strauss LG, Egerer G, Vasamilliette J, Schmitt T, Haberkorn U et al (2010b) Prediction of chemotherapy outcome in patients with metastatic soft tissue sarcomas based on dynamic FDG PET (dPET) and a multiparameter analysis. *Eur J Nucl Med Mol Imaging* 37:1481–1489
- Dimitrakopoulou-Strauss A, Strauss LG, Heichel T, Wu H, Burger C, Bernd L et al (2002) The role of quantitative (18)F-FDG PET studies for the differentiation of malignant and benign bone lesions. *J Nucl Med* 43:510–518
- Dimitrakopoulou-Strauss A, Strauss LG, Schwarzbach M, Burger C, Heichel T, Willeke F et al (2001) Dynamic PET ¹⁸F-FDG studies in patients with primary and recurrent soft-tissue sarcomas: impact on diagnosis and correlation with grading. *J Nucl Med* 42:713–720
- Epelbaum R, Frenkel A, Haddad R, Sikorski N, Strauss LG, Israel O et al (2013) Tumour aggressiveness and patient outcome in cancer of the pancreas assessed by dynamic ¹⁸F-FDG PET/CT. *J Nucl Med* 54:12–18
- Fletcher CDM, Bridge JA, Hogendoorn P, Mertens F (2013) WHO Classification of tumours of soft tissue and bone, vol 5, 4th edn. IARC Press, Lyon
- Fletcher CDM, Unni KK, Mertens F (2002) editors. WHO classification of tumours. Pathology and genetics of tumours of soft tissue and bone. IARC Press, Lyon, France
- Fujiwara T, Matsuzawa T, Kubota K, Abe Y, Itoh M, Fukuda H et al (1989) Relationship between histologic type of primary lung cancer and carbon-11-L methionine uptake with positron emission tomography. *J Nucl Med* 30:33–37
- Hicks RJ (2005) Functional imaging techniques for evaluation of sarcomas. *Cancer Imaging* 5:58–65
- Higuchi T, Kawaguchi K, Miyake K, Han Q, Tan Y, Oshiro H et al (2018) Oral recombinant methioninase combined with caffeine and doxorubicin induced regression of a doxorubicin-resistant synovial sarcoma in a PDOX mouse model. *Anticancer Res* 38:5639–5644
- Igarashi K, Kawaguchi K, Kiyuna T, Miyake K, Miyaki M, Yamamoto N et al (2018) Metabolic targeting with recombinant methioninase combined with palbociclib regresses a doxorubicin-resistant dedifferentiated liposarcoma. *Biochem Biophys Res Commun* 506:912–917
- Inai R, Shinya T, Tada A, Sato S, Fujiwara T, Takeda K et al (2015) Diagnostic value of Thallium-201 scintigraphy in differentiating malignant bone tumors from benign bone lesions. *Ann Nucl Med* 29:674–681
- Kanda Y (2013) Investigation of the freely available easy-to-use software 'EZR' for medical statistics. *Bone Marrow Transplant* 48:452–458. <https://doi.org/10.1038/bmt.2012.244>
- Keller S, Inai R, Sato S, Tada A, Adam G, Yamamura J et al (2017) *AJR Am J Roentgenol* 208:171–179
- Kobayashi H, Kotoura Y, Hosono M, Sakahara H, Hosono M, Yao ZS et al (1995) Diagnostic value of Tc-99 m (V) DMSA for chondrogenic tumors with positive Tc-99 m HMDP uptake on bone scintigraphy. *Clin Nucl Med* 20:361–364
- Kwee TC, Basu S, Cheng G, Alavi A (2010) FDG PET/CT in carcinoma of unknown primary. *Eur J Nucl Med Mol Imaging* 37: 635–644. <https://doi.org/10.1007/s00259-009-1295-6>
- Lapela M, Leskinen-Kallio S, Varpula M, Grenman S, Alanen K, Nagren K et al (1994) Imaging of uterine carcinoma by carbon-11-methionine and PET. *J Nucl Med* 35:1618–1623
- Lim CY, Ong KO et al (2013) *Cancer Imaging* 13:448–457. <https://doi.org/10.1102/1470-7330.2013.0036>
- Nakajima R, Abe K, Kondo T, Tanabe K, Sakai S (2016) Clinical role of early dynamic FDG-PET/CT for the evaluation of renal cell carcinoma. *Eur Radiol* 26:1852–1862
- Nomura Y, Asano Y, Shinoda J, Yano H, Ikegame Y, Kawasaki T et al (2018) Characteristics of time-activity curves obtained from dynamic 11C-methionine PET in common primary brain tumors. *J Neuro-Oncol* 138:649–658. <https://doi.org/10.1007/s11060-018-2834-4>
- Nuutinen J, Leskinen S, Lindholm P, Söderström KO, Nägren K, Huhtala S et al (1998) Use of carbon-11 methionine positron emission tomography to assess malignancy grade and predict survival in patients with lymphoma. *Eur J Nucl Med* 25: 729–735
- Okada Y, Nihashi T, Fujii M, Kato K, Okochi Y, Ando Y et al (2012) Differentiation of newly diagnosed glioblastoma multiforme and intracranial diffuse large B-cell lymphoma using (11)C-methionine and (18)F-FDG PET. *Clin Nucl Med* 37(9):843–849. <https://doi.org/10.1097/RLU.0b013e318262af48>
- Okazumi S, Dimitrakopoulou-Strauss A, Schwarzbach MH, Straus LG (2009) Quantitative, dynamic ¹⁸F-FDG-PET for the evaluation of soft tissue sarcomas: relation to differential diagnosis, tumor grading and prediction of prognosis. *Hell J Nucl Med* 12:223–228
- Raphael B, Hwang S, Lefkowitz RA, Landa J, Sohn M, Panicek DM (2013) Biopsy of suspicious bone lesions in patients with a single known malignancy: prevalence of a second malignancy. *AJR Am J Roentgenol* 201:1309–1314. <https://doi.org/10.2214/AJR.12.10261>
- Rusten E, Rødal J, Revheim ME, Skretting A, Bruland OS, Malinen E (2013) Quantitative dynamic ¹⁸F-FDG-PET and tracer kinetic analysis of soft tissue sarcomas. *Acta Oncol* 52:1160–1167

- Schierz JH, Opfermann T, Steenbeck J, Lopatta E, Settmacher U, Stallmach A et al (2013) Early dynamic ^{18}F -FDG PET to detect hyperperfusion in hepatocellular carcinoma liver lesions. *J Nucl Med* 54:848–854
- Shinya T, Otomi Y, Dimitrakopoulou-Strauss A, Kubo M, Kondo M, Otomo M et al (2020) Preliminary clinical assessment of dynamic ^{18}F -fluorodeoxyglucose positron-emission tomography/computed tomography for evaluating the clinicopathological grade in patients with non-Hodgkin's lymphoma: a prospective study. *Nucl Med Commun* 41:26–33
- Shinya T, Otomi Y, Kubo M, Kinoshita M, Takechi K, Uyama N et al (2019) Preliminary clinical assessment of dynamic ^{18}F -fluorodeoxyglucose positron emission tomography/computed tomography for evaluating lymph node metastasis in patients with lung cancer: a prospective study. *Ann Nucl Med* 33:414–423. <https://doi.org/10.1007/s12149-019-01350-z>
- Shinya T, Sato S, Kunisada T, Inai R, Yanai H, Ozaki T et al (2015) Both a visual and a semiquantitative analysis for differentiating benign from malignant chondrogenic bone tumors using Tc-99 m (V) DMSA scintigraphy: a prospective study. *Nucl Med Commun* 36:802–807. <https://doi.org/10.1097/MNM.0000000000000328>
- van Waarde A, Jager PL, Ishiwata K, Dierckx RA, Elsinga PH (2006) Comparison of sigma-ligands and metabolic PET tracers for differentiating tumor from inflammation. *J Nucl Med* 47:150–154
- Zhang H, Yoshikawa K, Tamura K, Tomemori T, Sagou K, Tian M et al (2004) [(11)C]methionine positron emission tomography and survival in patients with bone and soft tissue sarcomas treated by carbon ion radiotherapy. *Clin Cancer Res* 10(5): 1764–1772
- Zhao S, Kuge Y, Yi M, Zhao Y, Hatano T, Magota K et al (2011) Dynamic 11C-methionine PET analysis has an additional value for differentiating malignant tumors from granulomas: an experimental study using small animal PET. *Eur J Nucl Med Mol Imaging* 38:1876–1886. <https://doi.org/10.1007/s00259-011-1865-2>

Publisher's Note

Springer Nature remains neutral with regard to jurisdictional claims in published maps and institutional affiliations.

Submit your manuscript to a SpringerOpen[®] journal and benefit from:

- Convenient online submission
- Rigorous peer review
- Open access: articles freely available online
- High visibility within the field
- Retaining the copyright to your article

Submit your next manuscript at ► [springeropen.com](https://www.springeropen.com)
